ACS APPLIED MATERIALS & INTERFACES

Research Article

Cite This: ACS Appl. Mater. Interfaces 2019, 11, 22817−22823

www.acsami.org

Interface-Dependent Radiative Lifetimes of Yb^{3+}, Er^{3+} Co-doped Single $NaYF_4$ Upconversion Nanowires

Xuezhe Zhou,[†,⊥] Xiaojing Xia,[‡,⊥] Bennett E. Smith,[§] Matthew B. Lim,[†] Alexander B. Bard,[§] Anupum Pant,[†] and Peter J. Pauzauskie*[,†,∥]

[†]Department of Materials Science & Engineering, [‡]Department of Molecular Science & Engineering, and [§]Department of Chemistry, University of Washington, Seattle, Washington 98195, United States

[∥]Fundamental & Computational Sciences Directorate, Pacific Northwest National Laboratory, Richland, Washington 99352, United States

Supporting Information

ABSTRACT: The development of upconversion nanomaterials for many photonic applications requires a detailed understanding of their radiative lifetimes that in turn depend critically on local environmental conditions. In this work, hexagonal (β-phase) sodium-yttrium-fluoride ($NaYF_4$) nanowires (NWs) were synthesized and substitutionally co-doped with a luminescent solid solution of trivalent erbium and ytterbium ions. A single-beam laser trapping instrument was used in tandem with a piezo-controlled, variable-temperature stage to precisely vary the nanowire's distance from the substrate. The spontaneous photoluminescence lifetime of the $^4S_{3/2} \rightarrow {}^4I_{15/2}$ transition from Er^{3+} ions was observed to change by >60% depending on the ions' separation distance from a planar (water/glass) dielectric interface. The $^4S_{3/2}$ state lifetime is observed to increase by a factor of 1.62 ± 0.01 as the distance from the quartz coverslip increases from ∼0 nm to ∼40 μm. Less significant changes in the luminescence lifetime (≤10%) were observed over a temperature range between 25 and 50 °C. The distance dependence of the lifetime is interpreted quantitatively in the context of classical electromagnetic coupling between Er^{3+} ions within the nanowire and the adjacent dielectric interface. We also demonstrate potential applications of the $NaYF_4$ NWs for both controlling and probing temperatures at nanometer scales by integrating them within a poly(dimethylsiloxane) composite matrix.

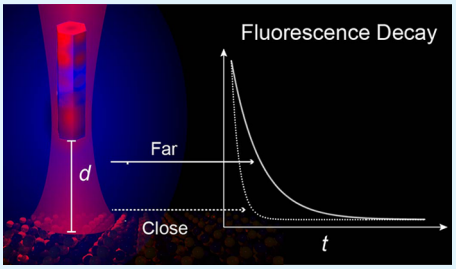

KEYWORDS: *upconversion, nanowires, radiative lifetime, optical density of states, laser tweezers, noncontact thermometry*

1. INTRODUCTION

Rare-earth-doped upconversion nanomaterials are suited for a wide range of applications[1] including color displays,[2] solar cells,[3,4] bioimaging,[5−8] drug delivery,[9] theranostics,[10] nanothermometry,[11] photodynamic therapy,[12] and cold Brownian motion.[13] These nanomaterials can be excited using near-infrared (NIR) radiation and emit bright, visible fluorescence.[14] A major challenge in conventional fluorescence imaging and labeling is that UV or visible excitation can cause autofluorescence. As a remedy, excitation using NIR light is a promising way to mitigate this challenge given biological specimens often are more transparent in NIR spectral windows. Among upconversion nanomaterials, hexagonal (β-phase) $NaYF_4$ has been studied as one of the most promising upconversion crystalline host lattices due to its biocompatibility, brightness, and photostability.[14,15] These methods are bright enough that confocal microscopy can be used to observe a single nanocrystal for super-resolution imaging.[16] In addition to being a good upconversion host material, $NaYF_4$ has been theoretically predicted to be an efficient host material for laser cooling with anti-Stokes fluorescence emission.[17] Recently, this has been demonstrated experimentally using single-beam laser tweezers.[18]

To improve upconversion performance, significant effort has been devoted to increasing the internal radiative quantum efficiency defined by the following equation

$$\eta = \frac{k_r}{k_r + k_{nr}} \quad (1)$$

Here, k_r is the radiative decay rate and k_{nr} is the nonradiative decay rate. Various approaches have been used to modify the radiative and nonradiative decay rates. As the size of an upconverting nanoparticle (UCNP) decreases, its lifetime shortens due to nonradiative decay caused by surface defects.[19,20] The surface can be modified by changing molecular ligands and/or by adding an inert, undoped inorganic shell as a coating, which can help reduce the surface defects and isolate them from emission quenchers, thereby increasing the luminescence.[21,22] Changes to the crystal lattice of the host may also modify the point group symmetry of the trivalent cations, which changes the local crystal field of the dopant ions, affecting photoluminescence (PL).[23] Additionally,

Received: January 18, 2019
Accepted: May 31, 2019
Published: May 31, 2019

DOI: 10.1021/acsami.8b17271
ACS Appl. Mater. Interfaces 2019, 11, 22817−22823

the dopant level in a UCNP can be optimized to prevent concentration quenching and tune PL wavelengths.[24] In addition to intrinsic material parameters, external environmental factors relating to electric and magnetic fields,[25,26] pressure,[27] temperature,[28] solvent,[29] and others can affect the radiative and nonradiative decay rates.

The predominant radiative decay pathways of rare-earth ions are intra-4f transitions, which can be estimated with the Judd–Ofelt theory.[30] One common experimental approach to characterize the optical properties of UCNPs is to prepare the sample on a glass substrate.[1,31] The total decay rate is the reciprocal of the transition's lifetime, which can be measured by fitting the fluorescence intensity decay profile. It has been reported recently[32] that the experimental radiative lifetime of nitrogen vacancy (NV) centers in diamond nanocrystals increases significantly when the NV centers are suspended within a silica-aerogel matrix ($n_{aerogel} \approx 1$) relative to NV centers on a planar glass substrate ($n_{SiO_2} \approx 1.3$). This observation has been interpreted in the context of the radiative decay rate depending critically on the classical local optical density of states (LDOS), which changes significantly as a function of distance from the dielectric interface.[32,33] Calculations using both semianalytical theory and finite-difference time-domain results have predicted that the emission rate for radiating dipoles increases as the particle approaches a planar dielectric interface, especially in the sub-100 nm distance range.[32−34] Similar experimental and theoretical results have been reported using single ions,[35] single dye molecules,[36] thin films,[37] and rare-earth ions doped within optical fibers.[38]

In this work, we use single-beam laser tweezers to position individual β-$NaYF_4$ nanowire (NW) cavities at precise distances from adjacent glass coverslips without changing any other variables within the local environment. Experimentally changing the LDOS (through tuning the NW cavity/interface separation distance) is observed to have a major impact on the experimentally measured lifetime of Er^{3+} ions emitting from the optically trapped nanowire cavity as discussed in more detail below.

2. RESULTS AND DISCUSSION

A low-cost, scalable hydrothermal synthesis approach is used to prepare β-$NaYF_4$ NWs that exhibit a hexagonal crystal structure, as shown in Figure 1a. The lattice structure of hexagonal β-$NaYF_4$ is not well defined. Three very similar space groups are proposed in the literature, and it is difficult to assign one structure to β-$NaYF_4$ due to its high variability.[39] Here, we compare our powder X-ray diffraction (XRD) patterns to previously reported structures and choose the $P\bar{6}$ space group, because it agrees best with our experimental diffraction data. Transmission electron microscopy (TEM) was used to measure the size and morphology of the NWs, as shown in Figure 1b. The diameter and length of individual NW cavities were measured. The average length and diameter were measured to be 1.68 μm and 0.25 μm, respectively. Figure 1c shows the dark field TEM image of a single nanowire. The crystallographic phase of the NWs was confirmed by XRD to be hexagonal (β-phase) $NaYF_4$ (PDF00-16-0334) as shown in Figure 1d.

A home-built single-beam NIR laser trapping instrument, as shown in Figure 2a, is used to perform lifetime spectroscopy experiments on single NW cavities. A 975 nm diode laser is

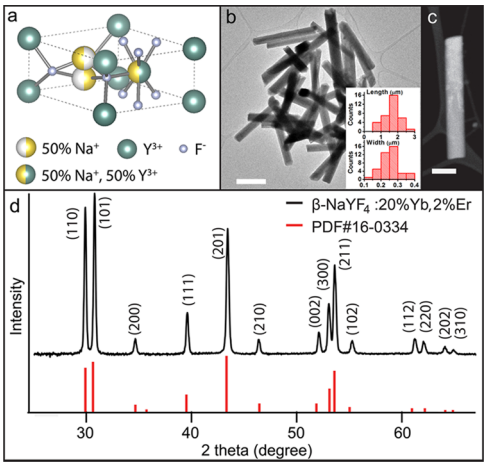

Figure 1. Synthesis and characterization of β-$NaYF_4$ nanowires. (a) Schematic of the hexagonal crystal structure of β-$NaYF_4$ with $P\bar{6}$ group symmetry. One of the internal atoms has 50/50 Na/Y split occupancy. The other is only Na, with some spatial delocalization (50% occupancy). (b) TEM image of $NaYF_4$ nanowires; scale bar = 1 μm. (c) Dark field TEM image of $NaYF_4$ nanowires; scale bar = 200 nm. (d) X-ray diffraction of ensemble $NaYF_4$ nanowires confirming the hexagonal phase structure.

focused by a 100× oil-immersion objective lens (NA = 1.25) down to a near-diffraction limited spot with a size of ~1.1 μm. The gradient optical force can trap a single NW in the focal plane, which enables three-dimensional (3D) manipulation of the NW by a piezo-controlled translation stage. The forward-scattered light is used to obtain the power spectral density (PSD) plot. A schematic graph for a characteristic, optically trapped NW is shown in Figure 2a inset. Following trapping, Er^{3+} ions within the nanowire are observed to emit bright PL (Figure 2c, middle) following energy transfer from Yb^{3+} ions.[40] The PL of a single NW collected by the same oil-immersion objective lens is filtered using a 750 nm short-pass filter and focused either on an avalanche photodiode (APD) or a liquid-nitrogen-cooled spectrometer. A 550 nm band-pass filter is placed before the APD to selectively collect emission from the $^4S_{3/2} \rightarrow {}^4I_{15/2}$ transition of Er^{3+} ions. The lifetime data are generated by processing the APD's time-dependent photovoltage signal, as described in the Methods section.

A color charge-coupled device (CCD) is used to monitor the in situ optical trapping process, which is shown in Figure 2c. The leftmost image in Figure 2c shows the bright-field image of a single $NaYF_4$ NW under Brownian motion in water. It is worth noting that the β-$NaYF_4$ NWs have a hexagonal crystal structure with an anisotropic index of refraction. As such, the lifetime may depend on the emission into different crystallographic *c*- ($\langle 001 \rangle$) and *a*- ($\langle 100 \rangle$) directions. Following optical trapping, the NW's long axis (crystallographic *c*-axis) aligns with the optical axis of the trapping laser due to radiation pressure.[41] Under these conditions, all of the variables that affect the $^4S_{3/2}$ state lifetime are held constant,[42] whereas the separation distance between the wire and interface is varied.

Forward-scattered laser radiation from the optically trapped NW creates a dynamic interference pattern within the microscope's back focal plane that can be detected with a high-speed silicon quadrant photodiode (QPD). The time-dependent photovoltage signal from the QPD is then Fourier-transformed to compute the resulting PSD. The diffusion

DOI: 10.1021/acsami.8b17271
ACS Appl. Mater. Interfaces 2019, 11, 22817−22823

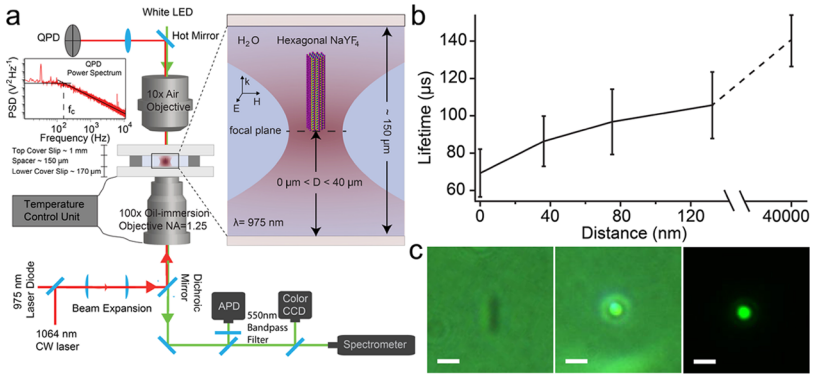

Figure 2. Schematic of laser trapping instrument for single-particle lifetime and fluorescence measurements. (a) An optically trapped $NaYF_4$ NW in an aqueous fluid chamber. (b) Er^{3+} $^4S_{3/2}$ state lifetime of an optically trapped $NaYF_4$ NW in the water at various distances from the quartz surface. (c) Left: the bright-field image of a $NaYF_4$ NW in Brownian motion, scale bar = 1 μm; Middle: the bright-field image of an optically trapped $NaYF_4$ NW using a 975 nm laser; Right: Image of an optically trapped $NaYF_4$ NW without illumination source showing green emission.

coefficient could be fitted from the PSD by a nonlinear least square fit. The piezo-stage is driven at a known frequency (32 Hz) and amplitude (100 nm) to enable spatial calibration of the PSD[43] from V^2/Hz to m^2/Hz to quantitatively measure the diffusion coefficient of the NW in the solution. As the trapped NW is brought close to the surface of the quartz, the diffusion coefficient gradually approaches zero due to hydrodynamic drag,[44] as shown in Figure S1. This onset of hydrodynamic drag is used to define the d = 0 nm point for distance-dependent lifetime measurements, and the piezo-stage together with the micrometer positioning stage were used to control the distance between the trapped NW and quartz surface from 0 to 40 μm.

As the trapping distance between the NW and the substrate is increased at room temperature, the $^4S_{3/2} \rightarrow {}^4I_{15/2}$ lifetime increases from 69 ± 12.8 to 139 ± 17.8 μs, as shown in Figure 2b. The average lifetime obtained from five different NWs were used to generate the plot in Figure 2b, where the error bars represent the standard deviation of the lifetime from the mean. The total PL lifetime is the reciprocal of the sum of the radiative and nonradiative decay rates. The laser power and temperature are held constant. To diminish the effect of laser heating on the substrate, a quartz substrate is used due to its low absorption coefficient at 975 nm,[45] which shows no obvious heating using ratiometric thermometry of Er^{3+} ions (see Figure S2). Therefore, it is reasonable to assume that the temperature-dependent nonradiative decay rate remains constant at various distances between the NW and the coverslip, and the only variable affecting the radiative lifetime is the distance between the NW and the dielectric interface.

Our primary interpretation for the drastic observed change in the lifetime is the classical increase in the LDOS at the coverslip.[32,33] The radiative decay rate is affected by the proximity of the emitting dipole to the dielectric interface. More precisely, when a dipole radiates near an interface, the decay rate is governed by the interference between the directly emitted electromagnetic waves and those reflected from the surface. Therefore, it is sensitive to the dipole's polarization and distance relative to the interface, which can result in significant changes in the radiative decay rate. According to the Judd–Ofelt theory, the radiative relaxation rate is determined by the transition's energy gap, electric and magnetic dipole moments, and the refractive index of the host material. The radiative decay rate is not strictly temperature-independent, because the refractive index above depends slightly on temperature. However, the temperature dependence of the radiative decay rate is much smaller compared to that of the nonradiative decay rate. The radiative decay rate is affected predominantly by the dielectric environment surrounding the dipole. In these experiments, we use a single-beam optical-trap to fix the orientation (dipole polarization) of a single NW and to control the separation distance between the NW and the dielectric interface, thereby altering the decay rate according to the interference mechanism mentioned above. The distribution in lifetimes at a given distance is attributed to the differences between individual NWs, including fluctuations in NW composition and morphology.[31,46]

Temperature also is known to have a significant impact on total lifetimes due to multi-phonon-mediated, nonradiative relaxation mechanisms. Figure 3a shows the measured temperature-dependent lifetime trend of optically trapped NWs at a distance of roughly 40 μm away from the substrate. At this distance, we assume that the substrate's effect on the lifetime may be neglected. The temperature of the solution is

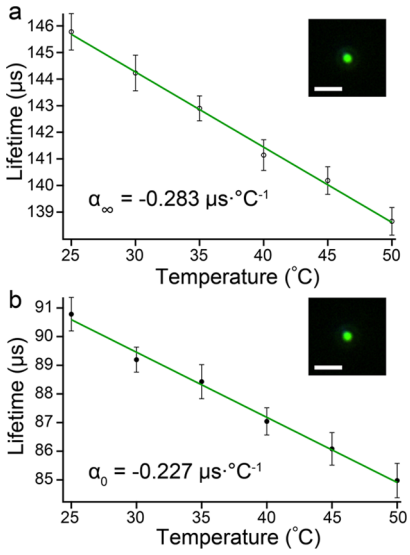

Figure 3. Temperature-dependent Er^{3+} $^4S_{3/2}$ state lifetime of a single optically trapped $NaYF_4$ NW in water. (a) $NaYF_4$ NW trapped 40 μm away from quartz surface. Inset: photoluminescence from the trapped NW; scale = 2 μm. (b) $NaYF_4$ NW trapped at the quartz surface. Inset: photoluminescence from the trapped NW; scale = 2 μm.

DOI: 10.1021/acsami.8b17271
ACS Appl. Mater. Interfaces 2019, 11, 22817–22823

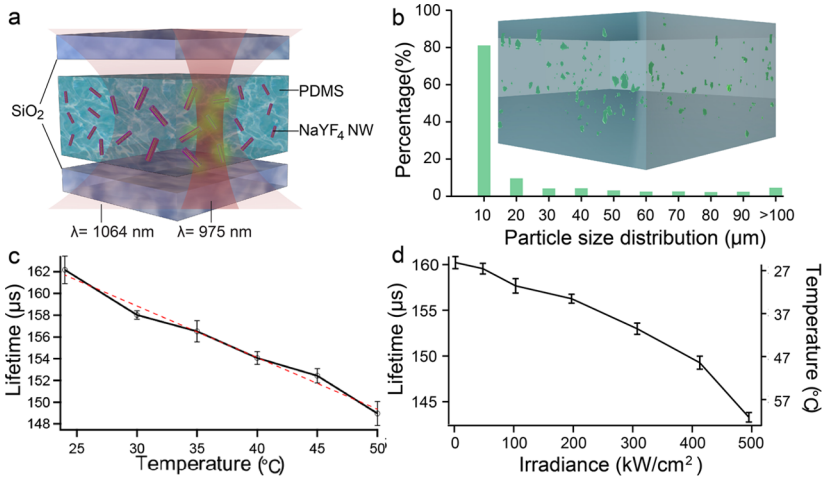

Figure 4. Optical thermometry of a PDMS/NW composite. (a) Schematic of an ensemble $NaYF_4$ embedded in the PDMS structure. (b) Confocal particle size histogram of $NaYF_4$ nanowires within the PDMS composite. (c) Temperature calibration using emission from the $^4S_{3/2} \rightarrow {}^4I_{15/2}$ transition from an ensemble of $NaYF_4$ NWs embedded in PDMS. (d) Irradiance-dependent heating of ensemble $NaYF_4$ NWs embedded in PDMS using a heating laser wavelength λ = 1064 nm.

controlled by a perfusion chamber with a resolution of 0.1 °C. As the temperature of the solution increases from room temperature, the $^4S_{3/2} \rightarrow {}^4I_{15/2}$ lifetime of the NW is observed to decrease by 10% over a temperature range of 25 °C. The decrease in the observed lifetime with temperature can be attributed to an increase in the nonradiative decay rate. Additionally, the impact of changing temperature on the lifetime is observed to be significantly smaller in comparison with changing the distance between the NW and the water/coverslip interface.

We define below a temperature-dependent parameter, α, to further quantify the effect of NW/coverslip separation distance on the observed total decay rate. In particular, the parameter α is defined as the derivative of the total lifetime with respect to temperature

$$\alpha = \frac{d\tau}{dT} = \frac{d(k_r + k_{nr})^{-1}}{dT} = -(k_r + k_{nr})^{-2}\frac{dk_{nr}}{dT} \quad (2)$$

where $\tau = \frac{1}{k_r + k_{nr}}$ is the total excited state lifetime, k_r is the temperature-independent radiative decay rate, and k_{nr} is the temperature-dependent nonradiative decay rate. The observed decrease in the lifetime with increasing temperature is observed to be linear over a total temperature range of 25 °C. Least squares fitting is used to quantify the slope α_∞ = −0.283 μs/°C, where the "∞" subscript indicates the NW is far from the water/coverslip interface. Identical measurements were made with the same NW located at the water/coverslip interface with α_0 = −0.227 μs/°C, where the "0" subscript indicates that the wire is located at the interface.

If the distance between the NW and coverslip is held constant during measurements of α, then this definition of α provides an experimental route to quantify the change in the radiative decay rate as a function of distance from the coverslip interface. The ratio of α coefficients from the same optically trapped NW both far from and near to the coverslip is given as

$$\frac{\alpha_\infty}{\alpha_0} = \left(\frac{k_0 + k_{nr}}{k_\infty + k_{nr}}\right)^2 \quad (3)$$

where k_0 is the spontaneous radiative decay rate when the NW is on the substrate and k_∞ is the spontaneous radiative decay rate when the NW is far away (∼40 μm) from the substrate. Here, we assume that $\frac{dk_{nr}}{dT}$ is the same for α_∞ and α_0, because the nonradiative decay rate does not depend on the distance between NW and the coverslip. The nonradiative decay is a result of the interaction of lanthanide ions with their surrounding microenvironment. The process of nonradiative relaxation depends on the energy gap between electronic states, the frequency of local phonon modes, and temperature.[47] The external electromagnetic environment, such as the NW/coverslip separation distance, does not affect nonradiative relaxation. This ratio can be used to calculate a lower bound for the change in the radiative decay rate as a function of distance from the coverslip. From the experimental data presented in Figure 3, we calculate the following values, α_∞ = −0.283 μs/°C and α_0 = −0.227 μs/°C, yielding the ratio $\frac{\alpha_\infty}{\alpha_0}$ = 1.15. Assuming $k_{nr} \rightarrow 0$, a lower bound for the substrate's effect on the radiative decay rate may be calculated using eq 3 implying

$$\frac{k_0}{k_\infty} \geq \sqrt{\frac{\alpha_\infty}{\alpha_0}} = \sqrt{\frac{0.283}{0.227}} = 1.12 \quad (4)$$

Given that k_{nr} is unaffected by the planar dielectric interface, the minimum amount that the radiative decay rate can increase is 1.12 times the rate for a single NW close to the substrate. When $k_{nr} > 0$, the ratio of radiative decay rates will be greater than 1.12.

In addition to quantifying the change in the radiative decay rate, the temperature-dependent $^4S_{3/2} \rightarrow {}^4I_{15/2}$ transition lifetime of Er^{3+} can be used for noncontact optical thermometry. Yb^{3+}- and Er^{3+}-co-doped $NaYF_4$ nanocrystals have been studied extensively for ratiometric nanothermometry, due to the existence of thermally coupled $^2H_{11/2}$ and $^4S_{3/2}$ energy levels. During ratiometric thermometry, an optical spectrometer is used to collect spectra that are postprocessed to measure temperatures with nanoscale spatial precision. In contrast, the lifetime-based method presented here requires only a low-cost and compact APD to collect a time-dependent

DOI: 10.1021/acsami.8b17271
ACS Appl. Mater. Interfaces 2019, 11, 22817−22823

photovoltage that can be fit using an exponential function in real-time to enable rapid, local temperature measurements. Due to their ability to manipulate particles in three dimensions, optical tweezers are well-suited to probe thermal gradient profiles, for example, surrounding a cell.[48−50] A precise calibration of the temperature-dependent lifetime change is shown in Figure 3 and clearly demonstrates it is possible to measure the temperature of single upconverting nanowires at physiological temperatures, where the change in the lifetime is linear with the temperature.

To further demonstrate the utility of NW lifetime thermometry, we embed upconverting NWs in an optically transparent poly(dimethylsiloxane) (PDMS) composite, as shown in Figure 4a. We use a pulsed 975 nm laser to probe the temperature and a 1064 nm laser to heat the sample. As 1064 nm is below the transition energy of Yb^{3+}, it will minimize upconversion. The uniformity and size distribution of NWs inside of the PDMS are observed using a 3D reconstruction made from confocal images of the composite (Figure 4b). We use a temperature-controlled stage and calibrate the lifetime of the NW ensemble within the composite at different temperatures. We measure a thermal coefficient $\alpha_{PDMS} = -0.475\ \mu s/°C$ (Figure 4c). The larger α coefficients between NWs in PDMS vs water could be due to the increased coupling between Er^{3+} ions and C−H bonds within PDMS. When the 1064 nm laser is co-aligned with the 975 nm laser spot, its power is increased to heat up the composite, and we can measure the temperature using ratiometric thermometry of the Er^{3+} fluorescence following laser excitation at λ = 975 nm maintained at a constant power. As the irradiance of the 1064 nm laser is increased from 0 to 495 kW/cm^2, the local temperature of the PDMS composite can be tuned from 300 K up to 336 K (Figure 4d), which is in the temperature range of many physiological processes. This dual laser beam system can potentially be applied in microfluidic systems for noncontact local temperature control and probes or in the design of future polymer composite cladding materials for radiation balanced lasers.[51]

3. CONCLUSIONS

We have presented a detailed investigation of how the presence of a dielectric interface impacts the total luminescence lifetime of single upconverting nanowires. We found that the lifetime changes significantly and predictably as a function of the NW's distance from the water/glass interface. This is of particular interest in developing new materials and methods for scanning probe microscopy, noncontact optical thermometry, secure quantum communication protocols, and radiation balanced lasers.[51] Beyond the investigation of single NW cavities, we have also studied the lifetime of NWs embedded within a PDMS composite. In the future, β-$NaYF_4$ NWs may be incorporated within polymeric composites to provide an optical approach for both controlling and measuring local temperature profiles with potential applications in the development of radiation balanced lasers.

4. METHODS

4.1. Hydrothermal Synthesis of $NaYF_4$ NWs. The following synthesis was performed after minor modifications to ref 18. Analytical grade sodium hydroxide, sodium fluoride, and oleic acid were used directly in the synthesis without any further purification. Milli-Q deionized (DI, 18.2 MΩ) water was used for each synthesis. Yttrium chloride, ytterbium chloride, and erbium chloride were of 99.999% purity and were purchased from Sigma-Aldrich. The RE chlorides were dissolved in 18.2 MΩ DI water to a concentration of 1 M. Two solutions were initially prepared. In the first solution, solution A, 0.78 mL of 1 M YCl_3, 0.2 mL of 1 M $YbCl_3$ and 0.02 mL of 1 M $ErCl_3$ were added to 2 mL of DI water and 8 mL of ethanol. Oleic acid (3 mL) and 0.23 g of NaOH were then added while stirring. The second solution, solution B, consisted of 0.168 g of NaF dissolved in 3 mL of DI water and 3 mL of ethanol. After each solution was stirred separately for 30 min, solution B was added to solution A dropwise while stirring vigorously. After 30 min, the mixture was transferred into a 23 mL Teflon-lined autoclave and heated hydrothermally at 220 °C for 5 h. After the autoclave cooled to room temperature, particles were isolated by washing and centrifuging with water and ethanol 3 times each. A white powder was obtained by drying the product in the air at 60 °C for 12 h.

4.2. $NaYF_4$ Embedded in PDMS. $NaYF_4$ (40 mg) was vigorously stirred with 50 mL of SYLGARD 184 silicone elastomer base for 10 min, and then the mixture was sonicated for 20 min. Then, 5 mL was transferred to a 10 mL tube to which 0.5 mL of the SYLGARD 184 silicone elastomer curing agent was added to form the final mixture. The mixture was then placed in a desiccator under house vacuum for 20 min to remove any gas bubbles in the mixture. The clear mixture (0.5 mL) was dropcast on a 1 in. wide, No. 1 thickness glass coverslip. It was then spin-coated at 100 rpm for 2 min, followed by 500 rpm for 2 min. The spin-coated coverslip was then heated in an oven at 70 °C for 12 h to achieve the $NaYF_4$ embedded PDMS.

To measure NW lifetime, a Tektronix function generator was used to modulate a Thorlabs LDC 220 laser-diode voltage controller. A 200 Hz repetitive rate and 1 ms pulse width waveform were applied to the laser diode. To ensure power stability of the laser during lifetime collection, the laser-diode output signal and APD voltage signal were both collected through a digital acquisition card to a computer and analyzed through a home-built LabVIEW code. The energy of each laser pulse was defined as the integration area of each pulse signal. The starting point for fitting the lifetime decay curve is chosen as the 99.99% diminished laser energy. To collect data from only the $^4S_{3/2}$ emission, a 550 ± 10 nm band-pass filter was used in place of the 750 nm short-pass filter. The APD intensity signal was fitted with double-exponential terms to get a lifetime value.

■ ASSOCIATED CONTENT

Supporting Information

The Supporting Information is available free of charge on the ACS Publications website at DOI: 10.1021/acsami.8b17271.

NW-coverslip contacting point determination; PSD corner fitting; ratiometric thermometry and fluorescence fitting (PDF)

■ AUTHOR INFORMATION

Corresponding Author

*E-mail: peterpz@uw.edu.

ORCID

Matthew B. Lim: 0000-0001-6129-9876
Anupum Pant: 0000-0002-6253-8418
Peter J. Pauzauskie: 0000-0002-1554-5949

Author Contributions

⊥X.Z. and X.X. contributed equally to this work. X.Z., B.E.S, X.X., M.B.L., and P.J.P. designed and performed experiments, analyzed data, prepared figures, and co-wrote the manuscript. A.B.B. and A.P. helped co-write the manuscript.

Notes

The authors declare no competing financial interest.

DOI: 10.1021/acsami.8b17271
ACS Appl. Mater. Interfaces 2019, 11, 22817−22823

■ ACKNOWLEDGMENTS

X.X. and P.J.P. gratefully acknowledge the support for single-nanowire lifetime measurements from the MURI:MARBLe project under the auspices of the AFOSR (#FA9550-16-1-0362). TEM characterization was performed by X.Z. with support from the US Department of Energy, Office of Science, Basic Energy Sciences, Division of Materials Sciences and Engineering, under Award KC020105-FWP12152. PNNL is operated by Battelle for the Department of Energy under contract no. DE-AC05-76RLO1830. Nanowire TEM characterization experiments were also supported by the US Department of Energy, National Center for Electron Microscopy at the Lawrence Berkeley National Laboratory (user proposal 4633). Part of this work was conducted at the Molecular Analysis Facility, a National Nanotechnology Coordinated Infrastructure site at the University of Washington, which is supported in part by the National Science Foundation (grant ECC-1542101), the University of Washington, and the Institute for Nanoengineered Systems.

■ REFERENCES

(1) Zhou, B.; Shi, B.; Jin, D.; Liu, X. Controlling Upconversion Nanocrystals for Emerging Applications. *Nat. Nanotechnol.* **2015**, *10*, 924−936.

(2) Park, B. J.; Hong, A.-R.; Park, S.; Kyung, K.-U.; Lee, K.; Jang, H. S. Flexible Transparent Displays Based on Core/Shell Upconversion Nanophosphor-Incorporated Polymer Waveguides. *Sci. Rep.* **2017**, *7*, No. 45659.

(3) Chen, X.; Xu, W.; Song, H.; Chen, C.; Xia, H.; Zhu, Y.; Zhou, D.; Cui, S.; Dai, Q.; Zhang, J. Highly Efficient $LiYF_4$:Yb^{3+}, Er^{3+} Upconversion Single Crystal under Solar Cell Spectrum Excitation and Photovoltaic Application. *ACS Appl. Mater. Interfaces* **2016**, *8*, 9071−9079.

(4) Shariatdoust, M. S.; Frencken, A. L.; Khademi, A.; Alizadehkhaledi, A.; van Veggel, F. C.; Gordon, R. Harvesting Dual-Wavelength Excitation with Plasmon-enhanced Emission from Upconverting Nanoparticles. *ACS Photonics* **2018**, *5*, 3507−3512.

(5) Mor, F. M.; Sienkiewicz, A.; Forro, L.; Jeney, S. Upconversion Particle as a Local Luminescent Brownian Probe: A Photonic Force Microscopy Study. *ACS Photonics* **2014**, *1*, 1251−1257.

(6) Chen, G.; Shen, J.; Ohulchanskyy, T. Y.; Patel, N. J.; Kutikov, A.; Li, Z.; Song, J.; Pandey, R. K.; Agren, H.; Prasad, P. N.; Han, G. Alpha-$NaYbF_4$:Tm^{3+}/CaF_2 Core/Shell Nanoparticles with Efficient Near-Infrared to Near-Infrared Upconversion for High-Contrast Deep Tissue Bioimaging. *ACS Nano* **2012**, *6*, 8280−8287.

(7) Chen, Z.; Zheng, W.; Huang, P.; Tu, D.; Zhou, S.; Huang, M.; Chen, X. Lanthanide-Doped Luminescent Nano-Bioprobes for the Detection of Tumor Markers. *Nanoscale* **2015**, *7*, 4274−4290.

(8) Ai, X.; Lyu, L.; Zhang, Y.; Tang, Y.; Mu, J.; Liu, F.; Zhou, Y.; Zuo, Z.; Liu, G.; Xing, B. Remote Regulation of Membrane Channel Activity by Site-Specific Localization of Lanthanide-Doped Upconversion Nanocrystals. *Angew. Chem., Int. Ed.* **2017**, *56*, 3031−3035.

(9) Yang, D.; Ma, P.; Hou, Z.; Cheng, Z.; Li, C.; Lin, J. Current Advances in Lanthanide Ion (Ln(3+))-Based Upconversion Nanomaterials for Drug Delivery. *Chem. Soc. Rev.* **2015**, *44*, 1416−1448.

(10) Chen, G.; Qju, H.; Prasad, P. N.; Chen, X. Upconversion Nanoparticles: Design, Nanochemistry, and Applications in Theranostics. *Chem. Rev.* **2014**, *114*, 5161−5214.

(11) Kucsko, G.; Maurer, P. C.; Yao, N. Y.; Kubo, M.; Noh, H. J.; Lo, P. K.; Park, H.; Lukin, M. D. Nanometre-scale Thermometry in a Living Cell. *Nature* **2013**, *500*, 54−58.

(12) Li, Y.; Tang, J.; Pan, D.-X.; Sun, L.-D.; Chen, C.; Liu, Y.; Wang, Y.-F.; Shi, S.; Yan, C.-H. A Versatile Imaging and Therapeutic Platform Based on Dual-Band Luminescent Lanthanide Nanoparticles toward Tumor Metastasis Inhibition. *ACS Nano* **2016**, *10*, 2766−2773.

(13) Roder, P. B.; Smith, B. E.; Zhou, X.; Crane, M. J.; Pauzauskie, P. J. Laser Refrigeration of Hydrothermal Nanocrystals in Physiological Media. *Proc. Natl. Acad. Sci. U.S.A.* **2015**, *112*, 15024−15029.

(14) Zhu, X.; Su, Q.; Feng, W.; Li, F. Anti-Stokes Shift Luminescent Materials for Bio-Applications. *Chem. Soc. Rev.* **2017**, *46*, 1025−1039.

(15) Sun, Y.; Feng, W.; Yang, P.; Huang, C.; Li, F. The Biosafety of Lanthanide Upconversion Nanomaterials. *Chem. Soc. Rev.* **2015**, *44*, 1509−1525.

(16) Liu, Y.; Lu, Y.; Yang, X.; Zheng, X.; Wen, S.; Wang, F.; Vidal, X.; Zhao, J.; Liu, D.; Zhou, Z.; Ma, C.; Zhou, J.; Piper, J. A.; Xi, P.; Jin, D. Amplified Stimulated Emission in Upconversion Nanoparticles for Super-Resolution Nanoscopy. *Nature* **2017**, *543*, 229−233.

(17) Hehlen, M. P. Crystal-Field Effects in Fluoride Crystals for Optical Refrigeration. In *Laser Refrigeration of Solids III*, 2010; p 761404.

(18) Zhou, X.; Smith, B. E.; Roder, P. B.; Pauzauskie, P. J. Laser Refrigeration of Ytterbium-Doped Sodium-Yttrium-Fluoride Nanowires. *Adv. Mater.* **2016**, *28*, 8658−8662.

(19) Vetrone, F.; Naccache, R.; Zamarrón, A.; Juarranz de la Fuente, A.; Sanz-Rodríguez, F.; Martinez Maestro, L.; Martín Rodriguez, E.; Jaque, D.; García Solé, J.; Capobianco, J. A. Temperature Sensing Using Fluorescent Nanothermometers. *ACS Nano* **2010**, *4*, 3254−3258.

(20) Qin, Y.; Yang, Z.; Yang, Y.; Zhou, D.; Qiu, J. Multi-Color Tunable Luminescence in Yb^{3+}, Er^{3+} Codoped $NaYF_4$ Nanocrystals Based on Size-Dependent. *Sci. Adv. Mater.* **2017**, *9*, 668−672.

(21) Fischer, S.; Bronstein, N. D.; Swabeck, J. K.; Chan, E. M.; Alivisatos, A. P. Precise Tuning of Surface Quenching for Luminescence Enhancement in Core-Shell Lanthanide-Doped Nanocrystals. *Nano Lett.* **2016**, *16*, 7241−7247.

(22) Wang, F.; Deng, R.; Wang, J.; Wang, Q.; Han, Y.; Zhu, H.; Chen, X.; Liu, X. Tuning Upconversion through Energy Migration in Core-Shell Nanoparticles. *Nat. Mater.* **2011**, *10*, 968−973.

(23) Wisser, M. D.; Fischer, S.; Maurer, P. C.; Bronstein, N. D.; Chu, S.; Alivisatos, A. P.; Salleo, A.; Dionne, J. A. Enhancing Quantum Yield via Local Symmetry Distortion in Lanthanide-Based Upconverting Nanoparticles. *ACS Photonics* **2016**, *3*, 1523−1530.

(24) Johnson, N. J. J.; He, S.; Diao, S.; Chan, E. M.; Dai, H.; Almutairi, A. Direct Evidence for Coupled Surface and Concentration Quenching Dynamics in Lanthanide-Doped Nanocrystals. *J. Am. Chem. Soc.* **2017**, *139*, 3275−3282.

(25) Hao, J.; Zhang, Y.; Wei, X. Electric-Induced Enhancement and Modulation of Upconversion Photoluminescence in Epitaxial $BaTiO_3$:Yb/Er Thin Films. *Angew. Chem., Int. Ed.* **2011**, *50*, 6876−6880.

(26) Bai, G.; Tsang, M.-K.; Hao, J. Tuning the Luminescence of Phosphors: Beyond Conventional Chemical Method. *Adv. Opt. Mater.* **2015**, *3*, 431−462.

(27) Wisser, M. D.; Chea, M.; Lin, Y.; Wu, D. M.; Mao, W. L.; Salleo, A.; Dionne, J. A. Strain-Induced Modification of Optical Selection Rules in Lanthanide-Based Upconverting Nanoparticles. *Nano Lett.* **2015**, *15*, 1891−1897.

(28) Zheng, S.; Chen, W.; Tan, D.; Zhou, J.; Guo, Q.; Jiang, W.; Xu, C.; Liu, X.; Qiu, J. Lanthanide-Doped $NaGdF_4$ Core-Shell Nanoparticles for Non-Contact Self-Referencing Temperature Sensors. *Nanoscale* **2014**, *6*, 5675−5679.

(29) Würth, C.; Kaiser, M.; Wilhelm, S.; Grauel, B.; Hirsch, T.; Resch-Genger, U. Excitation Power Dependent Population Pathways and Absolute Quantum Yields of Upconversion Nanoparticles in Different Solvents. *Nanoscale* **2017**, *9*, 4283−4294.

(30) Hehlen, M. P.; Brik, M. G.; Krämer, K. W. 50th Anniversary of the Judd-Ofelt Theory: An Experimentalist's View of the Formalism and Its Application. *J. Lumin.* **2013**, *136*, 221−239.

(31) Zhou, J.; Liu, Q.; Feng, W.; Sun, Y.; Li, F. Upconversion Luminescent Materials: Advances and Applications. *Chem. Rev.* **2015**, *115*, 395−465.

(32) Inam, F. A.; Grogan, M. D. W.; Rollings, M.; Gaebel, T.; Say, J. M.; Bradac, C.; Birks, T. A.; Wadsworth, W. J.; Castelletto, S.; Rabeau,

DOI: 10.1021/acsami.8b17271
ACS Appl. Mater. Interfaces 2019, 11, 22817−22823

J. R.; Steel, M. J. Emission and Nonradiative Decay of Nanodiamond NV Centers in a Low Refractive Index Environment. *ACS Nano* **2013**, *7*, 3833−3843.
(33) Inam, F. A.; Gaebel, T.; Bradac, C.; Stewart, L.; Withford, M. J.; Dawes, J. M.; Rabeau, J. R.; Steel, M. J. Modification of Spontaneous Emission from Nanodiamond Colour Centres on a Structured Surface. *New J. Phys.* **2011**, *13*, No. 073012.
(34) Lukosz, W.; Kunz, R. E. Light Emission by Magnetic and Electric Dipoles Close to a Plane Interface. *J. Opt. Soc. Am.* **1977**, *67*, 1607−1615.
(35) Pomozzi, A.; Park, M.-K.; Kreiter, M. Ensemble Measurement of the Orientation-Dependent Variations in Chromophore Lifetimes Near a Dielectric interface. *Phys. Rev. B* **2009**, *79*, No. 165435.
(36) Vallée, R.; Tomczak, N.; Gersen, H.; van Dijk, E. M. H. P.; Garcíá-Parajó, M. F.; Vancso, G. J.; van Hulst, N. F. On the Role of Electromagnetic Boundary Conditions in Single Molecule Fluorescence Lifetime Studies of Dyes Embedded in Thin Films. *Chem. Phys. Lett.* **2001**, *348*, 161−167.
(37) Ribierre, J. C.; Ruseckas, A.; Shaw, P. E.; Barcena, H. S.; Burn, P. L.; Samuel, I. D. W. Thickness Dependence of the Fluorescence Lifetime in Films of Bisfluorene-Cored Dendrimers. *J. Phys. Chem. C* **2008**, *112*, 20463−20468.
(38) Snoeks, E.; Lagendijk, A.; Polman, A. Measuring and Modifying the Spontaneous Emission Rate of Erbium Near an Interface. *Phys. Rev. Lett.* **1995**, *74*, 2459−2462.
(39) Szefczyk, B.; Roszak, R.; Roszak, S. Structure of the Hexagonal $NaYF_4$ Phase from First-Principles Molecular Dynamics. *RSC Adv.* **2014**, *4*, 22526−22535.
(40) Auzel, F. Upconversion and Anti-Stokes Processes with f and d Ions in Solids. *Chem. Rev.* **2004**, *104*, 139−174.
(41) Borghese, F.; Denti, P.; Saija, R.; Iatì, M.; Maragò, O. Radiation Torque and Force on Optically Trapped Linear Nanostructures. *Phys. Rev. Lett.* **2008**, *100*, No. 163903.
(42) Kreiter, M.; Prummer, M.; Hecht, B.; Wild, U. P. Orientation Dependence of Fluorescence Lifetimes Near an Interface. *J. Chem. Phys.* **2002**, *117*, 9430−9433.
(43) Tolić-Nørrelykke, S. F.; Schäffer, E.; Howard, J.; Pavone, F. S.; Jülicher, F.; Flyvbjerg, H. Calibration of Optical Tweezers with Positional Detection in the Back Focal Plane. *Rev. Sci. Instrum.* **2006**, *77*, No. 103101.
(44) Schäffer, E.; Norrelykke, S. F.; Howard, J. Surface Forces and Drag Coefficients of Microspheres Near a Plane Surface Measured with Optical Tweezers. *Langmuir* **2007**, *23*, 3654−3665.
(45) Haro-González, P.; del Rosal, B.; Maestro, L. M.; Martín Rodríguez, E.; Naccache, R.; Capobianco, J.; Dholakia, K.; García Solé, J.; Jaque, D. Optical Trapping of $NaYF_4$:Er^{3+},Yb^{3+} Upconverting Fluorescent Nanoparticles. *Nanoscale* **2013**, *5*, 12192−12199.
(46) Zheng, W.; Huang, P.; Tu, D.; Ma, E.; Zhu, H.; Chen, X. Lanthanide-Doped Upconversion Nano-Bioprobes: Electronic Structures, Optical Properties, and Biodetection. *Chem. Soc. Rev.* **2015**, *44*, 1379−1415.
(47) Liu, G. Advances in the Theoretical Understanding of Photon Upconversion in Rare-Earth Activated Nanophosphors. *Chem. Soc. Rev.* **2015**, *44*, 1635−1652.
(48) Rodríguez-Sevilla, P.; Zhang, Y.; Haro-Gonzalez, P.; Sanz-Rodriguez, F.; Jaque, F.; Sole, J. G.; Liu, X.; Jaque, D. Thermal Scanning at the Cellular Level by an Optically Trapped Upconverting Fluorescent Particle. *Adv. Mater.* **2016**, *28*, 2421−2426.
(49) Alaulamie, A. A.; Baral, S.; Johnson, S. C.; Richardson, H. H. Targeted Nanoparticle Thermometry: AMethod to Measure Local Temperature at the Nanoscale Point Where Water Vapor Nucleation Occurs. *Small* **2017**, *13*, No. 1601989.
(50) Wetzel, F.; Roenicke, S.; Mueller, K.; Gyger, M.; Rose, D.; Zink, M.; Kaes, J. Single Cell Viability and Impact of Heating by Laser Absorption. *Eur. Biophys. J.* **2011**, *40*, 1109−1114.
(51) Bowman, S. R.; Jenking, N. W.; O'Connor, S. R.; Feldman, B. Sensitivity and Stability of a Radiation-Balanced Laser System. *IEEE J. Quantum Electron.* **2002**, *38*, 1339−1348.

DOI: 10.1021/acsami.8b17271
ACS Appl. Mater. Interfaces 2019, 11, 22817−22823